

Tina Memo No. 2000-004

Short Version published in: JMRI, 10, 4, 550-562, 1999. Appendix added with recent developments.

A Fast Model Independent Method for Automatic Correction of Intensity Non-Uniformity in MRI Data.

E. Vokurka, N. Thacker and A. Jackson.

Last updated
7 / 2 / 2002



Imaging Science and Biomedical Engineering Division,
Medical School, University of Manchester,
Stopford Building, Oxford Road,
Manchester, M13 9PT.

1 ABSTRACT

A novel non-parametric approach for correcting intensity non-uniformity in magnetic resonance (MR) data in an image volume is described. This model is based on smooth shifts in intensity within homogeneous materials and does not require radio frequency (RF) coil, tissue class models, or optimisation. The advantage of this computationally fast method is that it can be applied early in quantitative analysis while being independent of pulse sequence and insensitive to pathological processes. This algorithm has been tested on both real and simulated data. Application to tissue segmentation and functional MR imaging has shown a marked improvement in quantitative analysis. See Appendix B for a summary of modifications to this algorithm since publication.

2 BACKGROUND

Historically, the emphasis on the development of magnetic resonance imaging (MRI) has been on the production of easily interpreted, high contrast, noise free diagnostic images. Recently, the medical physics community has begun to examine the extent to which MRI can provide quantitative information to investigate physiology and structure. The motivation for the non-uniformity correction algorithm presented below has been an interest in the use of multi-spectral MR data for quantitative analysis and measurement of tumour tissue. Most tissues are relatively homogeneous and should display a high degree of intensity uniformity throughout a given volume. This offers the potential of automatic and accurate structure determination for a wide variety of clinical tasks.

However, in the interest of obtaining low noise, high contrast images, some MR scanners often make undocumented adjustments to the amplification and digitisation of the RF image signal. These hardware adjustments can vary between the z-plane (phase encode) slices of a volume image and between scans for a particular patient. A similar problem exists for within slice variation due to sensitivity effects, particularly for surface receiver.

All magnetic resonance images suffer from signal intensity non-uniformity to some extent causing a smooth drift of average intensity across constant regions of tissue. Radio frequency (RF) coil asymmetry, gradient-driven eddy currents, pulse sequence parameters, and overall patient anatomy all potentially contribute to this gain drift [3].

Many simple analysis techniques, requiring repeatable measurements, are impossible or impeded due to changing MR scanner calibration and patient and coil positioning over time. This has potential implications across areas of MR image analysis, including perfusion measurements, functional imaging, segmentation, and co-registration. Some analysis techniques are designed to cope with these effects, but often the approach is to ignore the problem and assume that consequent errors are small.

While average intensity non-uniformities of 10-30% in standard head coil data will affect visual diagnosis minimally, the accuracy of quantitative procedures such as co-registration, segmentation, and functional imaging can be significantly affected [4][8]. It is essential to develop a fast, robust method of compensating for un-modelled gain changes across an image volume, reducing systematic error in quantitative measurements.

Several attempts at providing a preprocessing volume gain correction algorithm have been presented in the literature. Fluid phantom models, while correcting for RF transmit and receive inhomogeneities, do not take into account patient anatomy and orientation [5]. Methods requiring tissue classification or modelling also require a level of expert supervision, including the majority of those classed as *automatic* [6]-[9].

A method has been recently developed, N3, [4] which uses optimisation to estimate the field correction assuming Gaussian intensity distortions. While it provides a genuinely automatic non-uniformity estimate, the N3 algorithm still falls short at several levels. Although trivial in most images, the foreground needs to be segmented from the background, thus making it difficult for intensity correction of regions of interest where the signal drops to noise level. The necessarily iterative nature of the N3 method introduces biases caused by non-uniform noise levels in the iterative images which are additive, not multiplicative. The approximately Gaussian nature of the field is only estimated in head coil data and therefore may not be accurate for different anatomical regions or levels of distortion. Subsampling of the image is necessary to reduce the computational time required for the algorithm.

Two techniques are described below for the correction of intensity non-uniformity effects based on the re-integration of well measured local derivatives and intensity ratios. Their accuracy has been tested test on simulated data sets. The techniques are fast and, unlike some recent techniques, make few assumptions regarding the expected functional form of gain distortions. The algorithms are designed to be robust and to reduce the anticipated effects tissue boundaries, image noise, and integral wind-up. Their use on real data sets has been demonstrated, illustrating the value of such a procedure on a wide range of quantitative MR image analysis problems.

3 MATERIALS AND METHODS

The statistical framework for the inter-slice non-uniformity correction algorithm is the identification of a smooth underlying trend in the data as distinct from additive noise or scene structure. If this multiplicative distortion can be reliably calculated in well measured regions, it is a relatively straightforward task to interpolate the observed trends across the entire image. For this work we assume that the image content is due to a mean regional tissue grey levels, g_t , a spatially varying multiplicative gain, $G(x, y)$ and additive noise $n(x, y)$. The resulting image intensity is therefore

$$I(x, y) = g_t G(x, y) + n(x, y). \quad (1)$$

The gain estimation algorithm is as follows:

- estimation of additive image noise
- estimation of normalised local intensity gradients $\frac{\partial I/\partial x}{I}$ and $\frac{\partial I/\partial y}{I}$
- estimation of smooth local derivatives using statistical averaging
- re-integration of derivatives to determine a ‘relative’ gain map $C(x, y)$
- computation of the ‘true’ gain map $G(x, y)$

This process will be described in detail below.

The algorithm for determining intra-slice intensity variation is based on the robust estimation of consistent slice-to-slice relative intensity shifts.

All components of the intensity non-uniformity algorithms described have been written in C on a Sun UltraSparc using LINUX. The method has been integrated into the TINA image analysis software and is available as open source [11]. The patient data was acquired using a Philips ACS-NT 1.5 Tesla scanner.

3.1 NOISE ESTIMATION

Before any intensity non-uniformity can be estimated, the level of noise in the image, σ_I , must be determined. A $(-1, 0, 1)$ template is implemented to estimate the gradient across a voxel in both x and y directions. The gradient histograms are iteratively windowed with respect to their width to remove outlying edge effects. The average standard deviation from the cropped gradient histograms provides a robust estimate of noise in a given image.

3.2 INTER-SLICE NON-UNIFORMITY CORRECTION

Smooth intensity variations within an acquisition slice are mapped using the weighted re-integration of relative intensity gradients. The noise in an individual slice is determined before a 3x3 median filter is passed over the voxels to remove outlier noise while maintaining gradient distortions and edges. A $(-1, 1)$ template has been used to estimate the intensity shift across adjacent voxels $\Delta_k(x, y)$. x and y are the in-slice voxel coordinates, and k is the gradient direction, x or y . An option of placing an upper limit in units of statistical edge significance, $n\frac{\sigma_L}{\sqrt{2}}$, on gradients is provided. This reduces edge strength effects in the final inhomogeneity mask for tissues with large partial volume regions (i.e. grey and white matter mixing in the brain). For head coil images studied, $n = 2$ appears sufficient. It has not been necessary to constrain the edges in any other anatomical image sequence studied. Once the gradients are determined, they are normalised to remove tissue dependency, g_t , within homogeneous regions. In the case of the x -direction we define

$$\begin{aligned} \Delta_x^{rel}(x, y) &= \frac{\partial G(x, y)/\partial x}{G(x, y)} = \frac{2\Delta_x(x, y)}{I(x, y) + I(x - 1, y)} \\ &= \frac{2(I(x, y) - I(x - 1, y))}{I(x, y) + I(x - 1, y)}. \end{aligned} \quad (2)$$

In order to determine a statistically meaningful estimate of local smooth, relative gain variations each normalised gradient value is weighted with the differential error derived from equation 2.

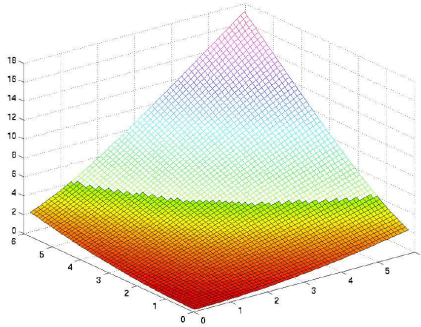


Figure 1: This surface shows weights calculated from two adjacent voxels with intensities in units of noise. The filled region lies below the weight limit of σ_{reg} . The significance of low weights is reduced by combining their gradient calculation with the constraint of minimum gradient with maximum error.

$$\sigma_x^{-2}(x, y) = \frac{(I(x, y) + I(x - 1, y))^4}{16\sigma_I^2(I(x, y)^2 + I(x - 1, y)^2)} \quad (3)$$

A conservative approach to boundaries between tissues and regions of low statistical accuracy has been taken. Voxels with low signal, $I(x, y) < \sigma_I$, or those with edges $> n\frac{\sigma_I}{\sqrt{2}}$, in images with large regions of partial volume, have this weight, $\frac{1}{\sigma_k^2}$, set to 0. No confidence is taken in the information available at these positions.

A further weighting factor takes into account the prior expected dependency of local gradients due to smoothness. The δ_k^{rel} images are passed through a smoothing filter S . Though the specific shape of the smoothing kernel is relatively arbitrary, two applications of an exponential IIR filter is a computationally efficient approximation to smoothing with a radially symmetric Gaussian filter. This filter has the characteristic of being a band pass filter in the Fourier domain and is thus a well posed method for enforcing smoothness on the reconstructed solution. The appropriately weighted mean estimate of smooth local relative gradient is given by

$$\Delta_x^S(x, y) = \frac{S \otimes \Delta_x^{rel} \sigma_x^{-2}(x, y)}{S \otimes \sigma_x^{-2}(x, y)} \quad (4)$$

where \otimes represents a 2D convolution. The weighting reduces the significance of poorly measured gradients during convolution, after which they are removed by division. For an image with uniform intensity in homogeneous tissue, equation 4 is zero for all voxels in a slice. This can be used as the basis for a regularisation term to provide increased mathematical stability. Δ_x^S becomes

$$\Delta_x^S(x, y) \Rightarrow \frac{S \otimes (\Delta_x^{rel} \sigma_x^{-2}(x, y) + 0_{reg})}{S \otimes (\sigma_x^{-2}(x, y) + \sigma_{reg}^{-2})} \quad (5)$$

The factor σ_{reg} is calculated at $I(x, y) = I(x - 1, y) = 3\sigma_I$ as in figure 1. This upper limit on the error constrains the effect of any voxel with large error in their gradient calculations. However, the bias introduced towards zero gradient in regions dominated by noise necessitates a limited number of iterations of the gain correction process in order to converge on the correct value of local gain variation.

Equation 5 should provide a map of the smooth intensity gradients in an image in the x direction. In order to produce a two dimensional image of the inhomogeneities, the x and y gradient maps are re-integrated to form the relative gain image, $C(x, y)$. The centre of the image, contained in the region of interest for most MR analysis, is used as a reference point of unity gain about which to construct the full solution.

Integration of noisy data sets can potentially lead to a problem generally referred to as an integral wind-up of error. We have designed a technique to attempt to control this process and improve statistical accuracy by making use of the redundant information available from both directions of re-integration. Integrated slopes along x and y axes originating from the centre of the image are calculated. The algorithm then integrates both clockwise around the quadrant boundary c_q and outwards from the centre c_o . The gradients along the axes are used to anchor the clockwise slope with the assumption that any integral windup is linear within a quadrant. We work with quadrants

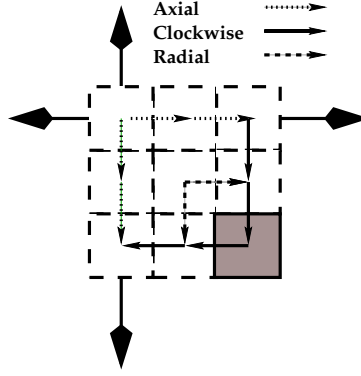


Figure 2: **Fig** Double re-integration paths for a voxel is shown (shaded). The coloured paths indicate multiple directions of integration. Each voxel uses the previous voxel as a reference point.

so that if any one part of the image is not correctable by a finite gain (due to very low signal levels) this will not affect the others. The boundary integration process can be written as

$$c_l = ls + \sum_0^l \Delta_l^S \quad (6)$$

where l is the position of the voxel in the quadrant and s is the correction derived from the axis gradient such that

$$c_o(0, y) - c_l(0, y) = 0 \quad (7)$$

Having gained this consistency, the two estimates of gain are then simply averaged (on an assumption of equal accuracy) at all points excluding the diagonals.

$$C(i, j) = (c_l(i, j) + c_o(i, j))/2 \quad (8)$$

A schematic of the re-integration is shown in figure 2.

The inverse of the exponential of the resulting inhomogeneity map provides the multiplicative correction to a given image (Appendix A).

At present the user needs to provide the algorithm with two values: a limit on edge strength and the size of the smoothing kernel. For images acquired with a head coil, an edge limit of $\frac{3\sigma_I}{\sqrt{2}}$ to safeguard against grey/white matter partial volume effects is sufficient. No other images studied appeared to need an edge strength limit. A smoothing kernel of 5% of the image size is a good rule of thumb across the images studied.

3.3 INTRA-SLICE INHOMOGENEITY CORRECTION

Segmentation studies have shown that the brain is dominated by regions of mixed white and grey matter tissues which contribute to inaccuracies in the location of the white matter peak. Slice-to-slice inhomogeneity correction methods for head coil images relying on white matter intensity distributions are marred by partial volume effects. Adjustments to the RF gain for individual slices in a volume, to optimise signal-to-noise ratio, cannot generally be expected to have a simple linear behaviour. The correction for intra-slice inhomogeneity presented below uses information gained from regions of relatively homogeneous tissue in contiguous or co-registered volumetric slices. It is applicable to any region of anatomy and any shape of gain drift.

For intra-slice inhomogeneity in a volume, the central image is used as a reference to which every other slice is corrected. A slice is always compared to an adjacent neighbour, creating a chain of relative correction factors. For time course studies, such as functional MRI, equivalent anatomical slices are processed.

A 3x3 median filter is passed over two adjacent images to reduce noise effects. The slices are thresholded on $3\sigma_I$ to remove the effect of noise. Edges are thresholded at $\frac{3\sigma_I}{\sqrt{2}}$, since edges are inconstant across adjacent images. With the poorly measured voxels masked, the natural log of the quotient of remaining intensities is taken to produce a symmetric distribution (see below).

$$\mathcal{F}_{i,j} = \ln \frac{I_{i,j}^{corr}}{I_{i,j}^{ref}} \quad (9)$$

$\mathcal{F}_{i,j}$ is binned in an odd number of statistically significant bins. For images larger than 128x128, 51 bins is sufficient. A parabola is fit to the heights, h_k , of the three central bins.

$$Corr = \frac{h_{c-1} - h_{c+1}}{2(h_{c+1} + h_{c-1}) - 4h_c} + C \quad (10)$$

C is the position of the central peak and $Corr$ is the correction to $\ln I^{corr}$. A perfectly uniform pair of images would produce $Corr = 0$. Multiplying the un-normalised image by \exp^{-Corr} brings the image closer to normalisation. Iteration of this process removes the significance of the parabolic assumption so that the correct solution is obtained provided only that the distribution is symmetrical. To reduce the effect of error accumulation, the correction factors are estimated for each adjacent slice pair before they are multiplied to normalise the volume to the central slice. The process is iterative, converging on a parabolic fit, symmetric around the central bin.

4 RESULTS

4.1 INTRA-SLICE STUDIES

Both patient and computer generated images have been used to test the 2D gain estimation algorithm. A checkerboard with 1% noise has been used in the intra-slice inhomogeneity studies (Figure ??). A double Gaussian distortion is used to increase intensity in regions by as much as 50%. The correction map from one application of the intra-slice algorithm is shown. The standard deviation of the bright regions in the corrected image is 3.67, while the average standard deviation of bright regions taken individually is 1.37 (c.f. $\sigma_I = 1.11$). Due to the isolation of the individual squares, the algorithm corrects the checkerboard in plateaus. Therefore while the overall non-uniformity is 3%, the local non-uniformity is of the order of noise at 1%. The double peaked corrected distribution illustrates the tight localised uniformity.

In addition to this geometric phantom, a phantom head coil image was generated from real data using a partial volume fitting method based on the principles of Bayesian labelling of MR data found in [10]. Using this technique it is possible to reconstruct a composite phantom image from tissue probabilities which is almost identical to the original scan. The brain phantom has been multiplied by a single Gaussian distortion varying the image intensity by 80%. Noise of 20% white matter signal is added. This severity of non-uniformity has been chosen to illustrate a worst case scenario, with the signal dropping to noise level. After 5 iterations, the correction map contains a maximum of 2% gain correction. The iterations are necessary due to the inhomogeneity of the tissue in the phantom brain.

Regions with white matter content above 85% are masked off to identify reasonably pure white matter voxels. The widths of the distorted, corrected, and original white matter distributions are compared in Figure 4. The standard deviation of the white matter distribution is combined with the calculated noise for a conservative estimate of the error of white matter identification. The error on the corrected image, $\sigma_c = 42$, is 68% of that of the distorted white matter peak, $\sigma_d = 61$, and 76% of the original distribution, $\sigma_o = 55$. The improvement on the original width is potentially due to the 10-30% gain drift found in most head coil images. Since the phantom was generated using probability fitting from real patient data, this gain drift has not been previously removed. The noise in the original image is measured at $\sigma_I = 45$, placing the error on the corrected white matter peak within the level of noise in the image.

Patient head coil images of Inversion Recovery, Variable Echo, T1, and TOF_angio sequences were tested with the algorithm and all converged to $\sim 2\%$ gain map correction within 5 iterations of the intra-slice algorithm. In addition to head coil data, surface coil shoulder, spine, choleca, skin, and orbit images were processed to check the potential of the improvement to visual diagnosis. All showed marked improvement after one iteration. An example of the improvement is shown in Figure 5.

4.2 INTER-SLICE STUDIES

The probabilistic brain phantom is also used in inter-slice studies. Identical slices are multiplied by a sinusoidal gains ranging from 50% to 150% intensity of the image. Random noise of 20% of white matter peak intensity is added to each of the images in the series. One iteration of the inter-slice correction varies by an average of 1.3% from the true gain correction. In addition to this phantom sequence, patient data from a T1 brain and shoulder

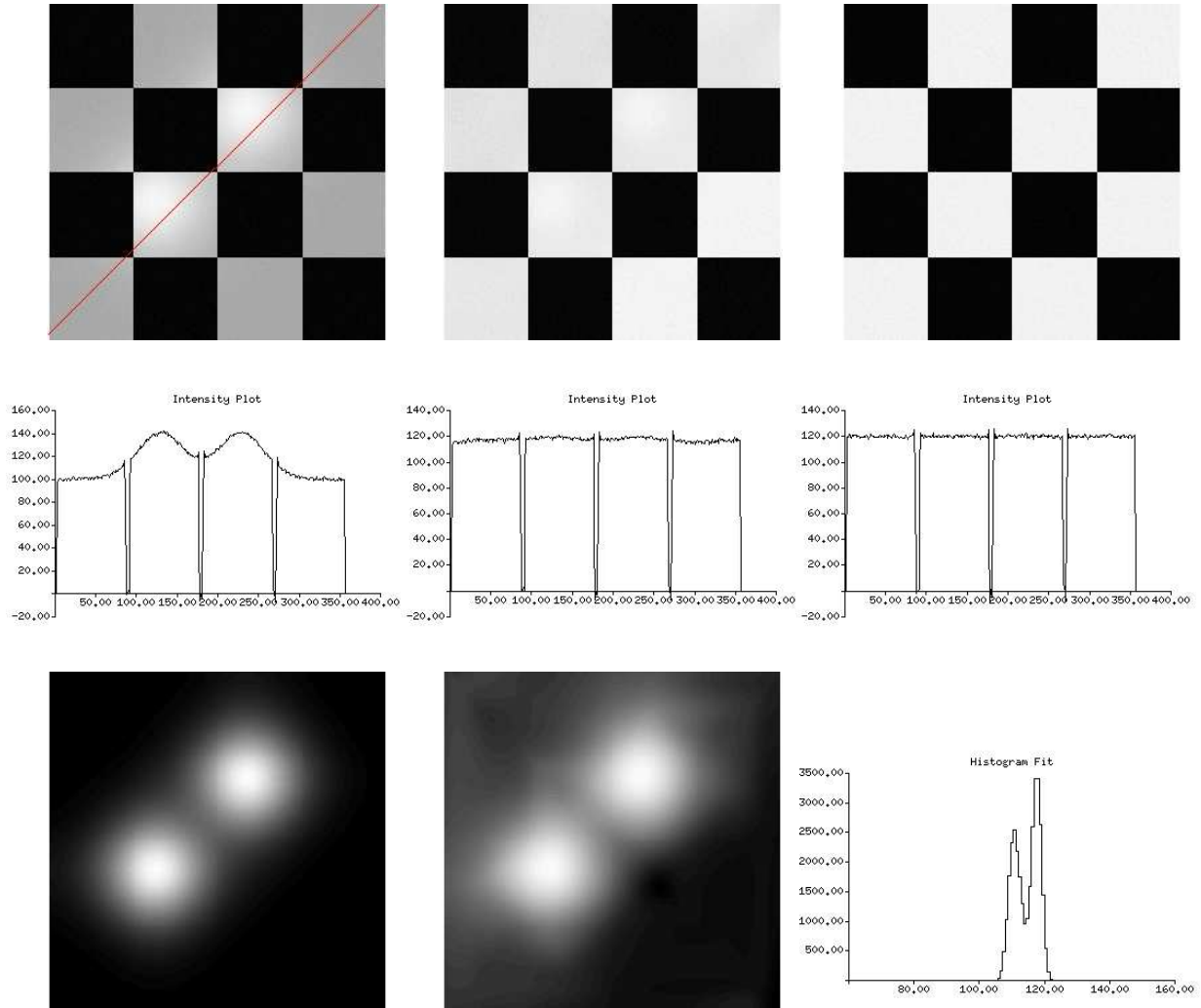


Figure 3: One iteration of the intra-slice inhomogeneity algorithm locally corrects for the distortion to the level of noise. a) deformed checkerboard, b) corrected checkerboard c) true checkerboard, d) e) and f) profiles across the diagonal of the image, g) true simulated inhomogeneity h) estimated inhomogeneity i) histogram of corrected image grey levels.

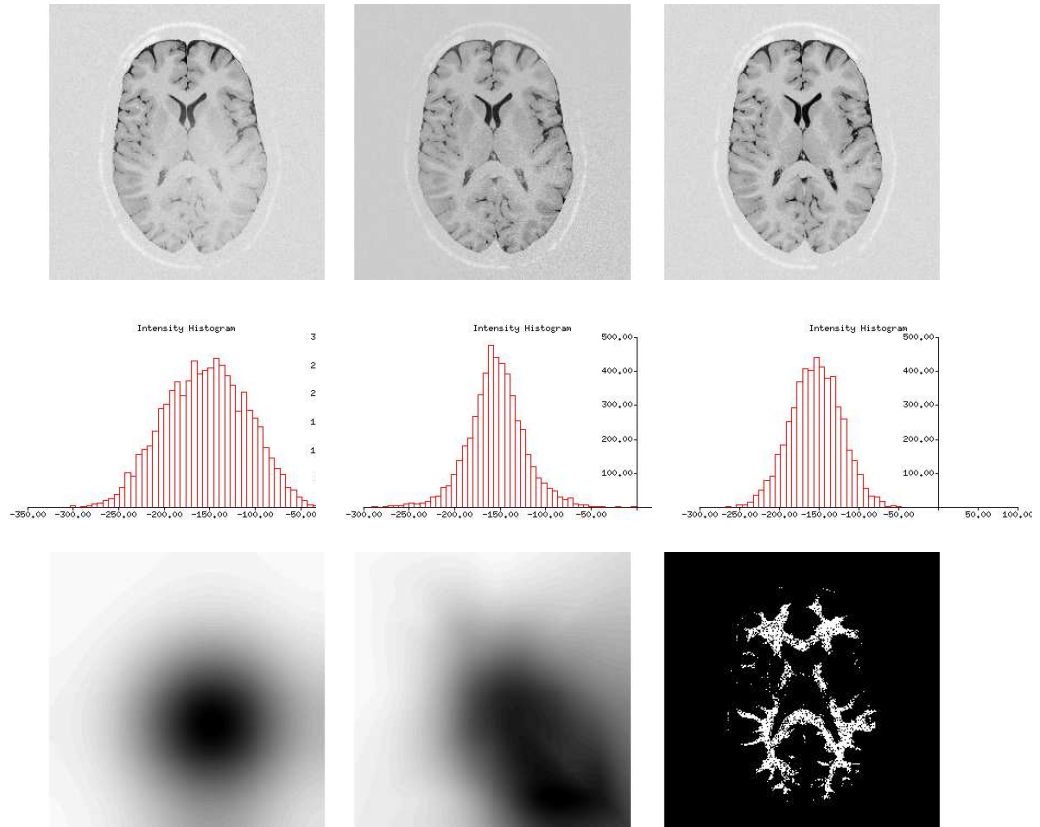


Figure 4: The distorted brain phantom white matter distribution is improved beyond the original distribution by the intra-slice algorithm. a) distorted image ,b) corrected image, c) original image, d) e) and f) corresponding histograms, g) applied distortion, h) estimated distortions, i) white matter segmentation.

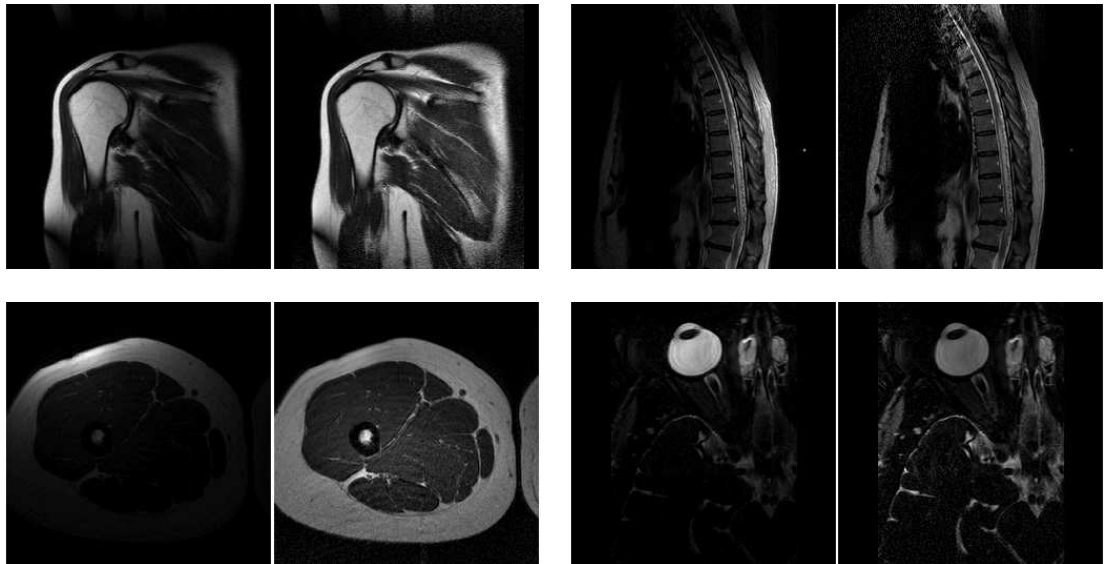


Figure 5: The intra-slice non-uniformity correction algorithm has the potential to improve visual diagnosis with surface coil images as demonstrated here with original and corrected images for a range of data types.

MR images are shown in Figure 6. After 4 iterations for the head coil data and 2 iterations of the shoulder data, the correction has converged.

In addition we have used this correction technique to adjust the relative normalisation of data in fMRI analysis. The conventional analysis approach involves correlation of a temporal data set with a specific stimulus response

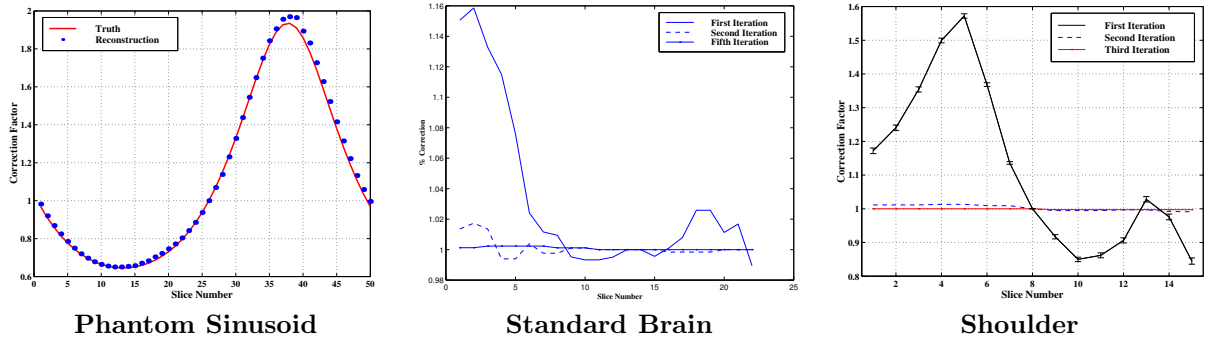


Figure 6: **FIG** The non-uniformity correction in z converges rapidly **PUT IN ERRORS**

function [1]. Random gain variations between dynamic acquisitions superimposes a random noise process on the grey level values, over and above the normal MR random noise mechanisms [Figure]. This effect is often corrected by use of an assumed linear model, which would be clearly inappropriate for this data [2]. This degrades the ability of a correlation analysis to distinguish between random noise and a genuine signal correlation. Correction for the random gain variation before correlation analysis has been found to improve the separation of signal from background by approximately 0.1 on a conventional Z score statistic on our scanner. This is statistically equivalent to increasing the length of the original temporal sequence by 50 %.

The computational requirements of both directions of normalisation is comparable. On a Sun Ultra5 workstation, each process requires 6 seconds CPU time per 256x256 slice. The time is linearly related to the square of the voxel dimensions in the image. Anatomical regions with large areas of homogeneous tissue require one pass of the intra-slice algorithm. Images with large fields of partial volume tissue (i.e. white and grey matter mixing in head coil images) may require iteration to achieve the same intra-slice accuracy. No more than 5 iterations were necessary on any head coil images studied to reduce the correction map to voxel adjustments of $\sim 2\%$. All image volumes studied converged to $< 1\%$ within 4 iterations of the inter-slice algorithm.

5 DISCUSSION

Our method for intensity non-uniformity correction is anatomically independent, not relying on tissue identification or any assumptions of RF coil modelling. No optimisation algorithm is implemented, and therefore, there is no risk of the correction bottoming out in a false minimum during the fit. No reduction in resolution is required to achieve a reasonable processing speed. From the studies performed, this method seems capable of correction a broad spectrum of non-uniformity for a wide range of anatomies, irrespective of the image's content. The assumptions on which this algorithm is designed are that MR images are composed of regions of homogenous tissues and discontinuous boundaries between them. This is sufficiently general that it would even be expected to be a reasonable approximation in pathology. We believe that the algorithm's success is simply due to careful use of appropriate statistical waiting during the computation process. This is used in order to control the effects of noise and sources of inaccurate data such as edges. We were also careful to try to design the technique in order to eliminate effects of integral wind-up of errors during integration. However, such effects have actually been found to be very small, and we believe that this is because the errors in local gradient estimation are actually anti-correlated in such a way that they largely cancel out during re-integration. Also, although the algorithm is iterative it has more in common with relaxation than optimisation and is not effected by local minima, converging stability within a few iterations.

At present, the inter-slice correction algorithm is fully automatic and requires no input beyond an initial automatic noise calculation. Again, we attribute the success of this algorithm to careful attention to statistical characteristics in the data and a design intended to engender statistical robustness. The assumptions of the algorithm only require that the distribution of estimates of relative gain between the two adjacent data sets be symmetrical around the peak in order to achieve correct convergence. This is a very weak assumption which may be expected to hold for a broad range of data sets. The intra-slice correction requires two input parameters which must be defined before the algorithm is implemented. The choice of smoothing kernel dimensions appears to be directly related to the size of the image itself. A limit on the edge cutoff appears only necessary in head coil images with white and grey matter mixing where there is little genuine homogeneous tissue. This also appears to be standard at $\sqrt{2}\sigma_I$. While present implementation of the algorithm in quantitative analysis may reveal limitations to these parameter choices, there is no need for expert supervision of the intra-slice correction at this time.

The algorithms mentioned are integrated in a freeware medical imaging package, TINA, [11]. Both the complete executable program and source code are available on the web.

Appendix A

An MR image is assumed to be composed of local regions of tissue R_t with mean grey level value g_t , a smooth multiplicative field, $G(x, y)$, and additive noise, $n(x, y)$. The resulting image intensity is therefore

$$I(x, y) = g_t G(x, y) + n(x, y). \quad (11)$$

Considering the noise-free case, the relative gain change in x (or y) is

$$\frac{\partial I / \partial x}{I(x, y)} = \frac{g_t \partial G(x, y) / \partial x}{(g_t G(x, y))} = \frac{\partial G / \partial x}{G(x, y)}. \quad (12)$$

Integration of equation 12 along any path S from s_0 to $s = (x, y)$ can be written as

$$\int_{s_0}^s \frac{\partial G / \partial s}{G_s} ds = \int_{s_0}^s \frac{\partial G}{G_s} = [\log(G_s)]_{s_0}^s. \quad (13)$$

Defining $\log(G_{s_0}) = 1$ gives the true gain variation relative to the starting point of the integration.

$$G(x, y) = G_s = \exp\left(\int_{s_0}^s \frac{\partial I / \partial s}{I_s} ds\right) \quad (14)$$

For a gain image limited to low frequencies the local estimates of relative gain change can be replaced with smoothed appropriately weighted mean estimates, Δ_x . This forms the basis of our computational approach to the integrated estimate of relative gain change, $C(x, y)$. The correction map to the estimated $G(x, y)$ is therefore

$$\bar{G}(x, y) = \exp^{-C(x, y)} \quad (15)$$

Appendix B

It has now been almost a decade since the algorithm presented in this paper was developed. Following publication we continued to apply the algorithm in analysis tasks and this inevitably drove a requirement for more accuracy and reliability. These developments were often subtle, and therefore could not become the focus of additional publications. As a consequence the software distributed from our web site (www.tina-vision.net) contains numerous embellishments to the algorithm as presented in this paper.

The first major development was made following the observation that the correction map was often very unstable in very low noise situations. Increasing the regularisation term often prevented accurate inhomogeneity estimates. Upon investigation we concluded that the simple (non-statistical way) that the integrability constraint was enforced did not take correct account of measurement imprecision. We therefore modified the algorithm to apportion the correction for integration consistency proportional to the accuracy of the estimated relative derivatives. This solved part of the accuracy issues, but geometric effects were still sometimes visible along the diagonal in images, as that was the direction in which the integration consistency check was least effective. In order to investigate this issue further an alternative algorithm was developed which implemented the same algorithm but applied the integration constraint along the diagonals of the image. We found that best results were obtained when we took an average of the two alternative correction maps thus obtained. We did not believe that this level of modification warranted an additional publication.

In our next piece of published work we decided to investigate the idea that information measures computed from image histograms, could be used as the basis for determining the field inhomogeneity. This was done in the context of trying to validate the overall effectiveness of the process ¹. We concluded that entropy measures are almost certainly inappropriate for this task (both empirically and theoretically). The theoretical foundation for use of entropy measures in estimation processes appears to as flawed, and a data set started from the know correction map

¹The work followed the rather negative evaluation of our algorithm published by Bostjan Likar (ICPR 2000), who erroneously applied our software to datasets which had both a multiplicative scaling and origin offset. When we asked for a copy of his software so that we could perform our own comparison he declined. His main claim was that the entropy based approach he had developed work best of all those algorithms tested. This led us to investigate the approach for ourselves.

moves to a radically different solution when optimising the entropy based information score. We also concluded however that the most sensible figure of merit for correction assessment, and the one consistent with our algorithm, is a robust measure of non-zero image slope (see Tina memo 2002-002). We therefore employed this alternative measure as a way to control the total level of correction applied to an image at each iteration of the algorithm. As the original version of the algorithm was effectively ‘open loop’, this improved both the convergence and reliability of the method.

Following these modifications the method was more reliable, but sometimes lacked stability in low signal images. For this reason we extended the method so that we could use two alternative MR images as input. The idea here is that by choosing two protocols where the field inhomogeneity is expected to be equivalent, we can supplement the lack of signal from low signal regions with inhomogeneity estimates from the other image. Clearly, the best pairing of such images would be those which had contrast reversal. The largely statistical design for the derivative estimate step for the original work made this extension relatively straight forward (Tina memo 2007-003). This approach is demonstrated with datasets in the downloads available from our website.

After a decade of modification, debugging and testing, We have found that the new version of the algorithm is quite reliable, except for those datasets with large quantities of partial volume data and therefore do not conform to the assumed data model. Unfortunately, this includes many of the thick slice brain scans acquired in clinical collaborations for which the method was originally intended. We have therefore often opted for acquisitions which minimise the effects of field inhomogeneity on segmentations (measured using this algorithm), or correction via other means. In particular, deviations from an assumed tissue density model can be determined directly using multiple acquisitions (see Tina memo 2004-009). We have not yet seen the technique work correctly on any images from a 3 Tesla scanner.

References

- [1] Bandettini P, Jesmanowicz A, Wong E C, Hyde J S., **Processing Strategies for Time Course Data Sets in Functional MRI of Human Brain**, M.R.M, 30, 161-173, 1993.
- [2] Brammer M L, Bullmore E T, Simmons A, Williams S C R, Grasby P M, Howard R J, Woodruff P W R, and Rabe-Hesketh S. **Generic Brain Activation Mapping in Functional Magnetic Resonance Imaging: A Non-Parametric Approach**, M.R.I., 15, 763-770, 1997.
- [3] Simmons A, Tofts PS, Barker GJ, Arridge SR, Sources of intensity non-uniformity in spin echo images, *Mag. Reson. Med.* vol. 32, pp. 121-128, 1994.
- [4] Sled JG, Zijdenbos AP, Evans AC, A nonparametric method for automatic correction of intensity non-uniformity in MRI data, *IEEE Trans. Med. Imag.*, vol. 17, no. 1, pp. 87-97, Feb. 1998.
- [5] Wicks DAG, Barker GJ, Tofts PS, Correction of intensity non-uniformity in MR images of any orientation, *Mag. Reson. Imag.* Vol. 11, pp. 183-196, 1993.
- [6] Özkan M, Dawant BM, and Maciunas RJ, Neural-network-based segmentation of multimodal medical images: A comparative and prospective study, *IEEE Trans. Med. Imag.*, Vol. 12, pp. 534-544, Sept. 1993.
- [7] Dawant BM, Zijdenbos AP, Margolin RA, Correction of intensity variations in MR images for computer-aided tissue classification, *IEEE Trans. Med. Imag.*, vol. 12, pp. 770-781, Dec. 1993.
- [8] Meyer CR, Bland PH, and Pipe J, Retrospective corrections of intensity inhomogeneities in MRI, *IEEE Trans. Med. Image.*, vol. 14, pp. 36-41, Mar. 1995.
- [9] Wells WM III, Grimson WEL, Kikiris R, and Jolesz FA, Adaptive segmentation of MRI data, *IEEE Trans. Med. Imag.*, vol. 15, no. 4, pp. 429-442, 1996.
- [10] Laidlaw DH, Fleischer KW, Barr AH, Partial-volume bayesian classification of material mixtures in MR volume data using voxel histograms, *IEEE Trans. Med. Imag.*, vol. 17, no. 1, 74-86, Feb. 1998.
- [11] <http://www.niac.man.ac.uk>